International Journal of Power Electronics and Drive System (IJPEDS)
Vol. 7, No. 4, December 2016, pp. 1294~1308
ISSN: 2088-8694, DOI: 10.11591/ijpeds.v7i4.pp1294-1308

Open-switch Fault-tolerant Control of Power Converters in a Grid-connected Photovoltaic System

B. Boudjellal, T. Benslimane
Laboratory of Electrical Engineering, University of M'sila, Algeria

Article Info

Article history:

Received Apr 14, 2016
Revised Nov 19, 2016
Accepted Dec 1, 2016

Keyword:

DC-AC three-phase converter
DC-DC power converter
Fault tolerance
Open switch fault
Photovoltaic (PV) System

ABSTRACT

This paper presents the study of an open switch fault tolerant control of a grid-connected photovoltaic system. The studied system is based on the classical DC-DC boost converter and a bidirectional 6-pulse DC-AC converter. The objective is to provide an open-switch fault detection method and fault-tolerant control for both of boost converter and grid-side converter (GSC) in a grid-connected photovoltaic system. A fast fault detection method and a reliable fault-tolerant topology are required to ensure continuity of service, and achieve a faster corrective maintenance. In this work, the mean value of the error voltages is used as fault indicator for the GSC, while, for the boost converter the inductor current form is used as fault indicator. The fault-tolerant topology was achieved by adding one redundant switch to the boost converter, and by adding one redundant leg to the GSC. The results of the fault tolerant control are presented and discussed to validate the proposed approach under different scenarios and different solar irradiances.

Corresponding Author:

Bilal Boudjellal,
Laboratory of Electrical Engineering,
University of M'sila,
Seat of the wilaya of M'sila, M'sila 28000, Algeria.
Email: bilal.boudjellal@univ-msila.dz

1. INTRODUCTION

Nowadays, photovoltaic (PV) systems are in an increasing demand as a renewable energy source, given that the natural resources of fossil and nuclear fuels are estimated to decrease drastically in this century, with the consequent raise of their costs. In addition, the need to reduce the pollution and the environmental concerns and sustainability problems related to an energy economy based on oil such as the climate warming [1]-[3]. Solar energy is available as a practically endless source, with no emissions, and with no risks for the environment.

Due to recent efforts in improving the performance, and in reducing degradation of PV cells, PV modules benefit from a high reliability [4] and their warranties last at least 20 years [5]. For such reasons, several countries have already applied this technology, together with other renewable energy sources such as the wind and hydraulic generation, to generate part of their present needs, and to meet the future energy requirements. Calculators, traffic lights and signalizations, water pumps, and warning systems are some of the most common small-size applications, but they are also suitable for high-power applications such as central power plants and electrification of remote areas [3]-[4].

There are three basic types of PV systems: grid-connected, standalone, and hybrid PV systems. They have specific applications and design concerns. High-power central power plants with a large number of PV modules in a huge area and householder PV systems are the most common practices to connect electric power produced from the PV cells to the grid. These systems are composed of many PV modules (which can have different arrangements), DC–DC converters with MPPT control, and inverters. In all these systems, DC–DC converters have a main role in conditioning the power produced by the PV generator. They track its maximum power point (MPP) at any climatic conditions and load demand, and provide the power interface to a dc bus, in the case of standalone (either only PV or hybrid) systems, or to an inverter, in the case of grid connected systems. Maximum power point tracking (MPPT) has been a main issue in many studies [6]-[11].

Connecting the renewable energy resources to a common DC bus provides several advantages as higher efficiency and reliability [12]-[13]. The DC bus is interfaced to the utility grid via DC–AC converter. Grid-connected three-phase converters are well documented in literature [14]-[15]. The grid-side converter (GSC) controls the DC bus voltage and reactive power transfer to the utility grid [12]. The control of GSC is bidirectional to facilitate the flow of power from the micro-grid to utility and vice versa instead of one-way operation as indicated in [13].

As in many other power applications, electrolytic capacitors and power switches are the most likely components to fail in power converters, because they are exposed to high mechanical and thermal stresses [16]-[17]. An excess of electrical and thermal stresses is the main cause for the failure of power switches, which can be classified as open-circuit and short-circuit faults [18]. Short-circuit fault protection is already a standard practice integrated in most power switches drives [19].

A failure in the DC–DC converter will affect the whole PV system and it might lead to its stoppage, since it is directly connected to the arrays [4]. Furthermore, a failure in the GSC can endangers the overall system and leads to it disconnecting [20]. Hence, to reduce the failure rate and to prevent unscheduled shutdown, real-time fault detection, isolation and compensation scheme is necessary to ensure continuity of service.

Recently, several papers have studied fault diagnosis methods in power electronic converters. Fault diagnosis in the power conversion stage of a grid-connected PV system is presented in [3]. A fault-tolerant strategy for a PV DC–DC converter is studied in [4]. The grid currents and root mean square currents are used for open-switch fault-tolerant control in a grid-side converter of a wind power generation system in [20]. A FPGA-based open- and short-circuit switch fault diagnosis for non-isolated DC–DC converters was proposed in [21]. A faults diagnosis in five-level three-phase shunt active power filter using output voltages to determine the open fault transistor is proposed in [22]. A fault-tolerant DC–DC converter topology based on redundancy is proposed in [23]. A fault diagnosis based on DC-link current pulse shapes of a ZVS DC–DC converter is proposed in [24]. And open switch fault tolerant six-legs AC-DC-AC in DFIG based WECS is presented in [25].

This paper presents a new developed approach fault-tolerant control of a grid-connected photovoltaic system. We examine the fault-tolerant control and the response of the PV system when an open-switch fault has occurred in one of the power switches in DC–DC converter or GSC converter. A brief description of the system including its modelling and control strategies are presented in sections 2, followed by a detailed explanation of the fault-tolerant strategy and the fault-detection method in sections 3 and 4, respectively. The results of the proposed methodologies are presented and discussed in section 5 to validate the proposed approach.

2. GRID-CONNECTED PHOTOVOLTAIC SYSTEM OVERVIEW

The studied system is shown in Figure 1. The PV array is connected through a unidirectional boost DC-DC converter with modular design. This modular converter transfer the available maximum power generated by PV array to DC bus. The generated PV power depends on the solar irradiation (*S*) and temperature (*T*). The DC bus is connected to the utility grid through a bidirectional 6-pulse PWM converter.

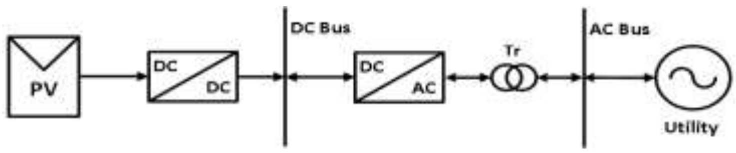

Figure 1. Grid-connected photovoltaic system

2.1. Modeling of Photovoltaic Solar Cell

Single-diode and two-diode circuit models are the most widely used for the PV solar cell. As the single-diode circuit model is accurate enough and used in many literature [3]-[8]-[12] it is adopted here. The model developed for the PV array is shown in Figure 2, it represents a complete array of PV cells by using a few equivalent components, which is convenient for faster simulations, and gives high accuracy in the behavior of the PV panels for different solar irradiances.

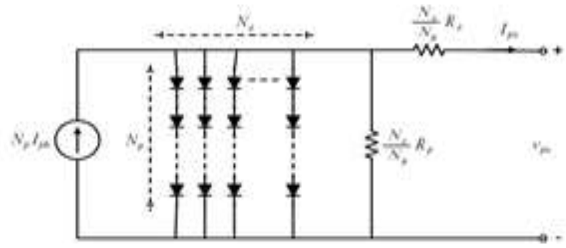

Figure 2. Equivalent circuit of a series-parallel array of photovoltaic cells

The I-V characteristic equation of the PV array is given as:

$$I_{pv} = N_p I_{ph} - N_p I_{sat}[e^{\frac{qF}{nkT}} - 1] - \frac{N_p F}{R_p}, F = \frac{v_{pv}}{N_s} + \frac{R_s I_{pv}}{N_p} \tag{1}$$

Where I_{ph} is the photocurrent of the cell and is given as:

$$I_{ph} = \frac{G}{1000}\left(I_{sc} + \alpha(T - T_r)\right) \tag{2}$$

The cell reverse saturation current, I_{sat} is given as:

$$I_{sat} = I_{rr}\left(\frac{T}{T_r}\right)^{\frac{3}{n}} e^{\frac{qE_g}{nk}\left(\frac{1}{T_r} - \frac{1}{T}\right)} \tag{3}$$

The inverse saturation current at the reference temperature I_{rr} is given by:

$$I_{rr} = \frac{I_{sc} - (V_{oc}/R_{sh})}{e^{(qV_{oc}/nkT_r)} - 1} \tag{4}$$

The PV array is based on BP-SX150 photovoltaic module. The PV system can deliver *40kW* to the grid at the maximum solar irradiance (1000W/ m^2). The parameters used in the simulation of the PV array are listed in Table 1.

Table 1. Solar cell module parameters

Symbol	Description	Value
G	Solar irradiance	*1000 W/m2*
Np	Number of cells in parallel	*34*
Ns	Number of cells in series	*576*
Isc	Short circuit current	*161.5 A*
Voc	Open-circuit voltage	*348 V*
Rs	Internal series resistance	*0.035* Ω
Rsh	Internal parallel resistance	*4 k*Ω
Eg	Band energy gap	*1.12 eV*
α	Temperature coefficient of Isc	*0.65×10-3*
n	Ideality factor	*1.62*
k	Boltzmann constant	*1.381×10-23 J/K*
q	Electron charge	*1.602×10-19 C*
T	Temperature of the PV cell	*298.15 °K*
Tr	Reference temperature	*298.15 °K*
Ipv	Rated output current	*147.9 A*
Vpv	Rated output voltage	*276*

2.2. Single-Ended Non-Isolated DC–DC Converters

Several topologies of DC-DC converters are used in classical power electronic applications. Non-isolated single-ended DC-DC converter is one family of DC–DC converters witch is consisting of: buck, boost, buck-boost, Ćuk, SEPIC, and dual SEPIC converters. These converters are increasingly being used in industrial applications such as in electric traction, electric vehicles, renewable dc sources, machine tools, and some other applications in distributed dc systems in ships, airplanes, and computers and in telecommunications.

Figure 3 shows a boost converter and its signals. There are two modes in one switching period T for the boost converter operating. In the first mode and during period of DT the switch S is turned on and the diode is off. Consequently, the input voltage is applied across the inductor and the inductor current i_L ramps up linearly, increasing the energy stored in the inductor. In the second mode and during period of (1−D) T the switch S is turned off and the stored energy in the inductor flows to the load and forces the diode to conduct. As a result, the inductor current $i_L$decreases.

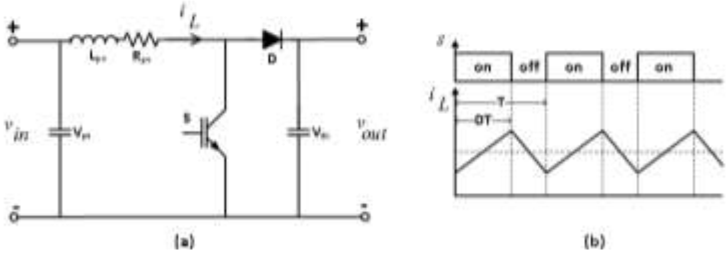

Figure 3. (a) Boost converter, and (b) Signals for a boost converter

2.3. Control of PV Source

The PV output power depends on the environmental conditions such as the solar irradiation (S) and temperature (T). In order to generate the maximum power from the PV array, its DC–DC converter is controlled using MPPT control technology. In this paper, Perturb and Observation (P&O) control method is adopted, which is the most widely useful method of MPPT control [6]-[8].

P&O is an iterative method of MPPT tracking. As shown in Figure 4, the PV array output voltage V_{pv}(n) and output current I_{pv} are measured periodically and the PV output power P (n) is calculated. Then the PV output power and voltage are compared with that of the previous sample power P (n-1) and voltages V (n-1), in order to get ΔP and ΔV.

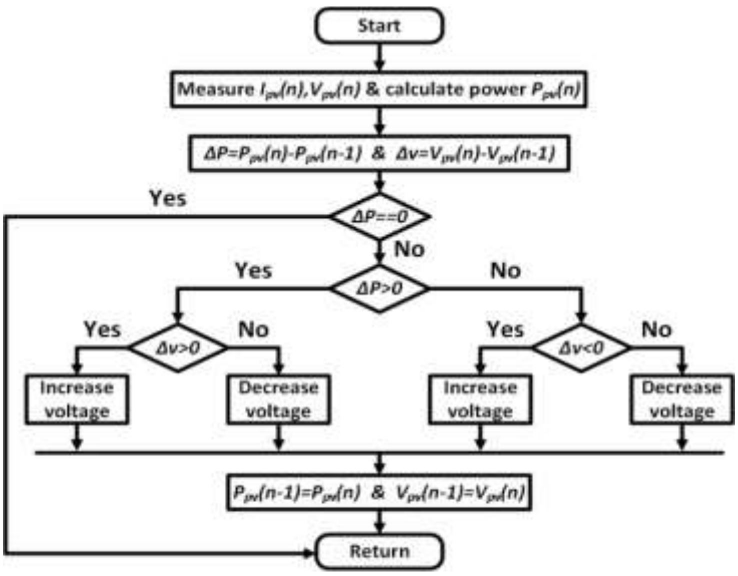

Figure 4. Flow chart of P&O algorithm

Then according to the sign of ΔP and ΔV, the reference voltage of the converter is changed to track MPP as summarized below [9]-[11].

a. If the value of ΔP is zero, the system is working at MPP and no change in reference voltage is required.
b. If the value of ΔP>0 and ΔV>0, the reference voltage is to be increased so as to reach MPP.
c. If the value of ΔP>0 and ΔV<0, the reference voltage must be decreased to reach MPP.
d. If the value of ΔP<0 and ΔV<0, the reference voltage is to be increased to reach MPP.
e. if the value of ΔP<0 and ΔV>0, the reference voltage this time is to be decreased to reach MPP.

The resulted error between the reference and measured voltages is manipulated using a PI controller to generate the duty cycle and consequently the PWM gate signal g_{pv} for the converter switch as illustrated in Figure 5.

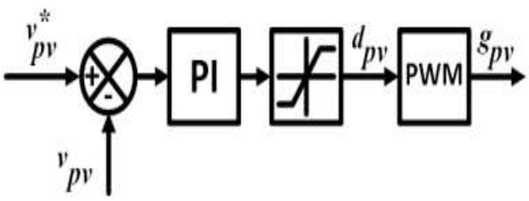

Figure 5. Block diagram of voltage control

2.4. Control of Grid-Side Converter

The DC bus is connected to the utility through The GSC, which is connected to the utility a through an RL filter to mitigate high frequency harmonics. The GSC is based on regulating the DC bus voltage and controlling the reactive power that is exchanged between GSC and the grid. The control of this converter is achieved by transforming the three phase quantities to (d, q) synchronously frame, so that the d-axis is aligned with the stator flux. So, the following relations are resulted:

$$\begin{cases} v_{fd} = 0 \\ v_{fq} = v_f \end{cases} \tag{5}$$

Through the following equations, the active power P_f and reactive power Q_f, can be calculated:

$$\begin{cases} P_f = v_f \, i_{fq} \\ Q_f = v_f \, i_{fd} \end{cases} \tag{6}$$

These equations show that independent active and reactive power control can be achieved. Figure 6 shows the model scheme of the field oriented control of GSC.

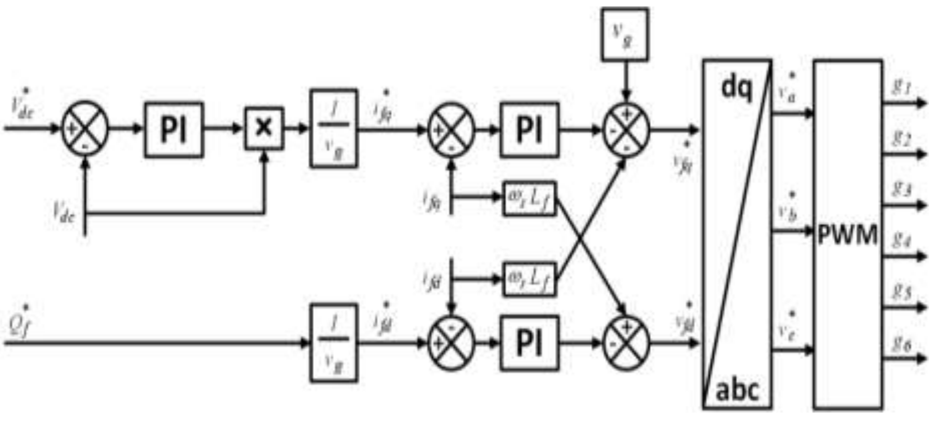

Figure 6. Model scheme of GSC vector control

3. FAULT-TOLERANT CONTROL

The studied grid-connected photovoltaic system contains a unidirectional boost DC–DC converter and a bidirectional 6-pulse PWM converter as it shows in Figure 7. Both of the two converters are vulnerable to semiconductors switches faults. The most common failures in semiconductors are open-circuit faults, gating faults, and short-circuit faults. These failures may happen due to external or internal events, such as: incorrect gate voltage, driver failure or electrical over stress (voltage or current) which may appear by electromagnetic pulses, electrostatic discharge, system transient, and lightning [18] [24] [25] [26].

Figure 7 shows the fault-tolerant topology with redundancy for the studied grid-connected PV system. The switching pattern for the DC–DC converter is defined by P&O control method and the switching patterns for the GSC are defined by vector control strategy. In healthy conditions, the outputs of the P&O and vector control are directly applied to the converters.

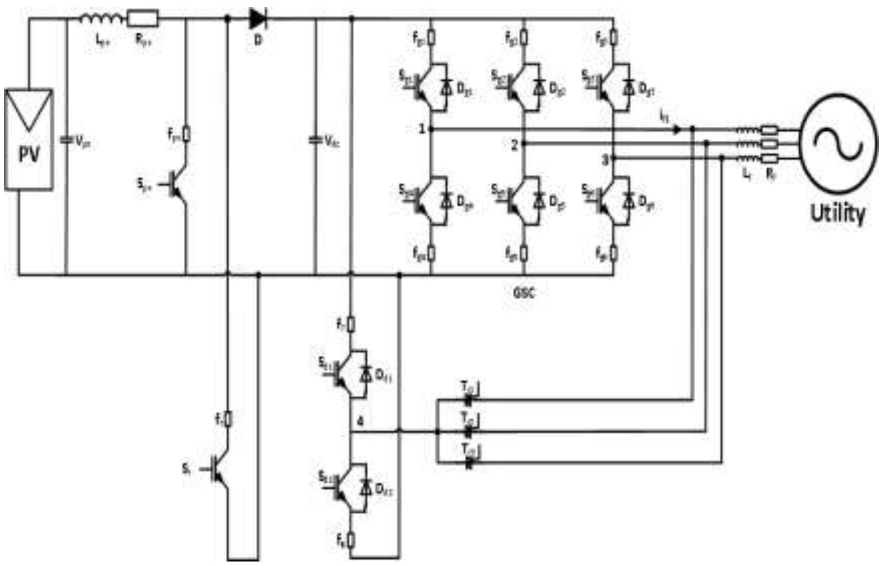

Figure 7. Fault tolerant converter topology for grid-connected PV system

3.1. Fault-Tolerant Control for the Boost DC-DC Converter

If a power switch failure occurred in the DC-DC converter, the fault detection method detects the fault occurrence and the switch S_{pv} will be replaced with the redundant switch S_r. The fusible f_{pv} is added in case of dangerous current occurred by short-circuit (SC). In summary, in an open-switch fault case on the DC-DC converter, the compensation is achieved by the following steps:

1. Detection of the fault,
2. Stop the switching orders of the switch S_{pv},
3. Use the switching orders of the switch S_{pv} to the switch S_r,
4. Stop the fault detection scheme.

3.2. Fault-Tolerant Control for the Grid-Side Converter

When a fault occurred in one of the semiconductors or drivers of the three-legs of the GSC, the fault detection method detects the fault occurrence and isolates the faulty leg. The faulty leg will be then replaced with the redundant leg (composed of the switches S_{d1} and S_{d2}). In case of a short-circuit fault, the faulty leg is isolated by very fast acting fuses; consequently, the short-circuit fault becomes an open-circuit. For these reasons, only open-switch fault will be studied for the GSC [25]. In summary, in an open-switch fault case on the three-legs of the GSC, the compensation is achieved by the following steps:

1. Detection of the faulty leg number k (k=1, 2, 3),
2. Stop the switching orders of the two switching drivers of the faulty leg,
3. Trigger the suited bidirectional switch T_{rk} of the faulty leg number k,
4. Use the switching orders of the faulty leg to the redundant leg,
5. Stop the fault detection scheme.

4. FAULT DETECTION METHODOLOGY
4.1. Fault Detection Method of DC-DC Converter

The proposed switch fault detection of the boost DC-DC converter is based on the form of the inductor current i_L, which is the same for the non-isolated single-ended DC-DC converters family, this fault detection method can be generalized to the other non-isolated single-ended DC-DC converters family. The proposed fault detection method does not require any additional current or voltage sensors in the system, which is interesting because additional sensors affect the reliability, cost, and weight of the system.

As shown in Figure 8, the fault detection method is based on two algorithms FDA1 and FDA2. The first algorithm FDA1 is faster than the second algorithm FDA2, but it is less robust at detecting an open-switch fault (OSF) for some cases. Although, the second algorithm FDA2 is more robust and efficient, however it is not as fast as the first algorithm FDA1.

Figure 9 shows the fault detection signals for the DC–DC converter when an OSF has occurred in different times T_{F1} and T_{F2}, we can observe that FDA1 is faster than FDA2 for the first fault case (OSF1). However, in the second case (OSF2), FDA2 is faster than FDA1 in detecting the fault. Both algorithms are described in the following.

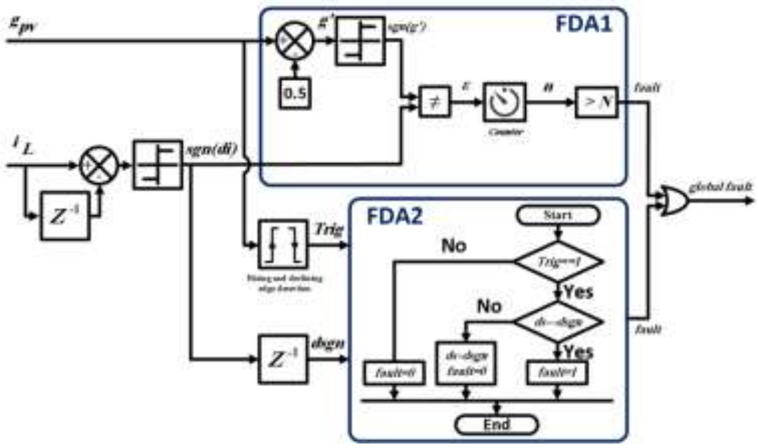

Figure 8. Fault detection algorithm for the DC–DC converter

The first fault detection algorithm FDA1 uses the form of the inductor current i_L, to be more accurate is uses the sign of the slope of i_L. The sign of the current slope sgn(di) is computed by calculating the derivative of the inductor current i_L and then pass it through a sign block. When the switch S_{pv} is turned on sgn(g')=1, i_L increases and sgn(di)=1. When the switch S_{pv} is turned off sgn(g')=-1, i_L decreases and sgn(di)=-1. If the two signals sgn(g') and sgn(di/dt) are different there is a switch failure.

In real time and as a result of non-ideal behavior of power switches and delays, the sgn(di) will be delayed in respect to sgn(g') and the error signal "ε" is set to "1" as shown in Figure 9. Hence, the power semiconductor switching, delays and dead times must to take into consideration to avoid false fault detections. Therefore, a counter block is added to assure the fault detection. In case of a switch fault, the error signal "ε" will be set to "1" and the counter "n" starts to count for enough time to assure the fault detection, otherwise if the error signal is set to "0" the counter will reset to zero "0". In case that the counter is greater than N it means that a switch fault occurred. The counting time must be longer than the overall delays caused by the sensors, drivers, controllers and switches:

$$N \cdot T_S > T_d \tag{7}$$

Where T_s is the sampling period and T_d is the total inherent delay.

Though, the FDA1 algorithm is very fast and can detect a fault within N sampling period, however it still depends on several parameters and there are some necessary criteria must to take into consideration to detect the fault successfully. These criteria can be summarized as:

$$\begin{cases} (DT - T_F) > N \cdot T_S \\ DT > N \cdot T_S \end{cases} \tag{8}$$

Where T_F is the fault occurrence time. FDA1 can detect the fault successfully if (8) are simultaneously satisfied. However, if these conditions are not satisfied, fault detection will fail. Considering (8), the OSF detection will fail for small values of D or in high-frequency switching. Because of these limits for fault detection, a second algorithm FDA2 is proposed.

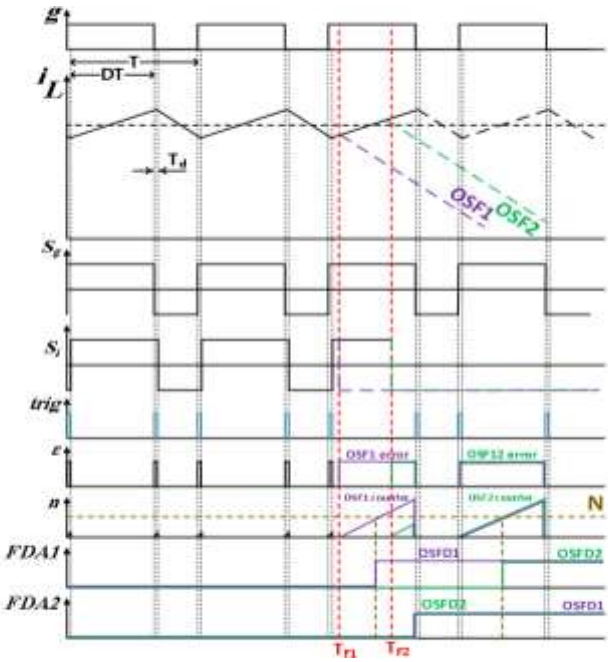

Figure 9. Fault detection signals for the DC–DC converter

The second fault detection algorithm FDA2 is bases on the form of the inductor current i_L as well. There is two states of the switch g_{pv} which are switch trigged on and switch trigged off, and by each pulse of "Trig", the inductor current i_L increases or decreases, and the slope sign of i_L changes by every Trig signals as shown in Figure 9. If the slope of i_L does not changes by the Trig signals it means that a switch failure has occurred. The second algorithm FDA2 as it shown in Figure 8 can be summarize by the following steps:

1. Detect the rising and declining edge "Trig" pulse;
2. Check if the slope sign of i_L changed by comparing the present i_L slope sign with the previous i_L slope sign;
3. If the slope sign of i_L changed then there is no fault and ds is set to equal dsgn;
4. If the slope sign of i_L did not change then a fault has occurred and fault is set to "1".

This algorithm is slower than the first algorithm, however it can detect the faults in any conditions, for any D and any switching frequency.

4.2. Fault Detection Method of GSC

The open-switch fault detection of DC–AC converter is based on the mean value of comparison between measured and estimated simple voltages v_k and v_{k_es} (k = 1, 2, 3) as illustrated in Figure 10. The estimated voltages can be expressed by:

$$\begin{bmatrix} v1 \\ v2 \\ v3 \end{bmatrix} = \frac{V\,dc}{3} \begin{bmatrix} 2 & -1 & -1 \\ -1 & 2 & -1 \\ -1 & -1 & 2 \end{bmatrix} \begin{bmatrix} S1 \\ S2 \\ S3 \end{bmatrix} \tag{9}$$

The mean value calculator it is the sum divided by the count time, in other words, add up all the numbers (data), then divide by time. However, in real time and cause of turn-on, turn-off, interlock dead, propagation time and time generated by the switches drivers, the voltage mean value error is not null. Therefore, to avoid false fault detections due to power semiconductor switching, we add two steps of detection. The first step is calculating the mean value of the voltage error signal and compare it with a threshold value h (Table 2). The second step is time delay to assure the fault detection it's done by comparing the threshold t_k with the time delay value τ, as shown in Figure 10. The resulting signal f_k from the fault detection diagram is used to isolate the faulty leg and start the compensation in fault case.

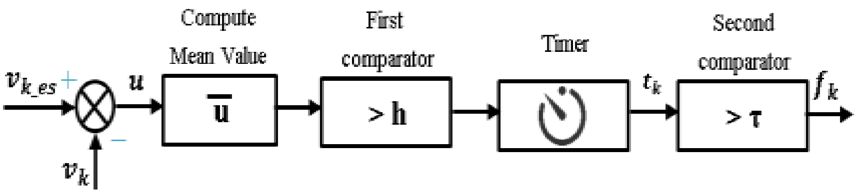

Figure 10. Block diagram of the proposed fault detection

Table 2 classified the faulty switch detection using each phase mean value threshold value.

Table 2. Faulty switch detection threshold

Faulty switch	Phase1	Phase2	Phase3
Sg1	$> h$	$< h$	$< h$
Sg2	$< h$	$> h$	$< h$
Sg3	$< h$	$< h$	$> h$
Sg4	$< h$	$> h$	$> h$
Sg5	$> h$	$< h$	$> h$
Sg6	$> h$	$> h$	$< h$

5. RESULTS AND ANALYSIS

The system model was developed and simulated in MATLAB/SIMULINK environment using the Simscape Power Systems toolbox for verifying the validity of the proposed fault-tolerant strategy and fault-detection methods. The system parameters are given in Table 3. The sampling period has been chosen to be equal to 1 µs. The pulse width modulation frequency is set to 10 kHz for the DC–DC converter and 5 kHz for the GSC. The GSC is connected to a three-phase utility grid of 380 v, 50 Hz. The nominal power of PV system is 40 kW at 1000 W/m^2 of solar irradiance and the temperature is assumed constant at the reference value. Fault detection methods parameters are N=40, h=10 and τ=1 ms.

Table 3. Simulation parameters

Variable	Value
Rpv	10 mΩ
Lpv	4 mH
Cdc	6000 µF
Lf	3 mH
Rf	5 mΩ

The solar irradiation S changes from 500 W/m^2 and 1000 W/m^2 as shown in Figure 11.

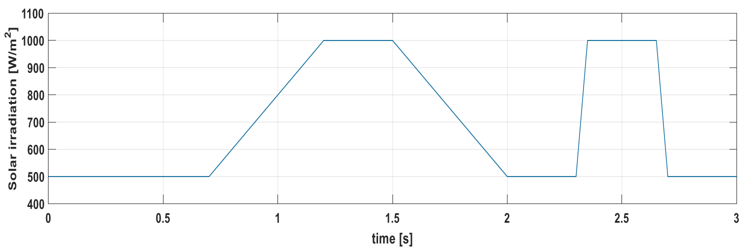

Figure 11. Solar irradiation (S)

The operation of the grid-connected photovoltaic system includes three cases of studies, a normal operation mode, an open-switch fault operation mode in both DC-DC converter and GSC.

5.1. Case study 1: Normal Operation Mode

In normal operation mode, the PV output power P_{PV} is varying between 20 kW and 40 kW accordingly to the value of S. It can be seen from Figure 12 that the P&O MPPT control method helps to generate the maximum power from the PV array by controlling the PV output voltage V_{PV}.

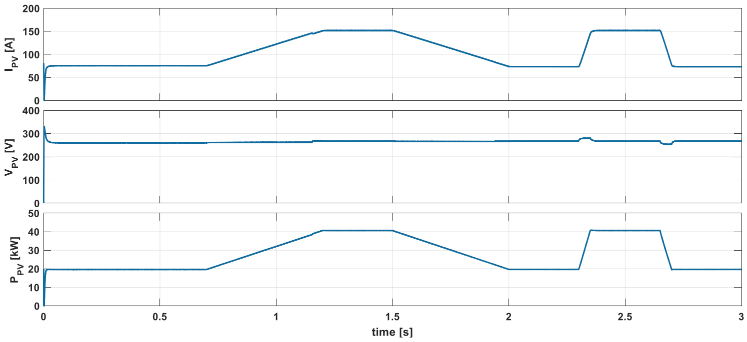

Figure 12. PV output current (I_{PV}), PV output power (V_{PV}) and PV output power (P_{PV})

Figure 13 show, the grid active power P_f, grid reactive power Q_f and DC bus voltage v_{dc}. The v_{dc} is well regulated to it reference (600 V) and sags are about 3% (18 V), however, it decreases and increases instantly when the P_f increases and decreases, respectively, and recovers quickly by the vector control strategy. The P_f is varying between -20 kW and -40 kW (the minus sign means it's a generated power) accordingly to the PV output power P_{PV}. The Q_f is fixed to zero value, to maintain the power factor at unity.

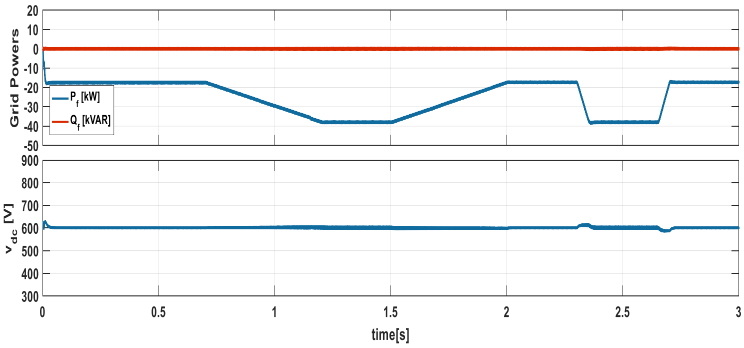

Figure 13. Grid active power (P_f), Grid reactive power (Q_f) and DC bus voltage (v_{dc})

5.2. Case Study 2: DC–DC Converter Open-Switch Fault Operation Mode

Figure 14 shows simulation results of studied system when an open-switch fault has occurred in DC-DC converter (switch S_{pv}) at t=2.2s without fault-tolerant topology. After the switch fault is occurred, both of PV output current I_{PV} and PV output power P_{PV} are drops to zero "0". As a result, the DC bus voltage v_{dc} drops as well, but recovers quickly by GSC. The grid active power P_f becomes positive, meaning that the power flows from the grid to the DC bus. In summary, we can conclude that a failure in the DC-DC converter will affect the whole PV system and lead to its stoppage since it is directly connected to the arrays. Figure 15 shows the DC–DC converter signals that used to detect the fault. This figure proves that the proposed fault detection method can detect open-switch fault in DC–DC converter (at time t=2.700042s). Figure 16 shows simulation results for the same fault when the proposed fault-tolerant topology is used. One can see that the PV system can still operate in nominal conditions even after open-switch fault is occurred in DC–DC converter.

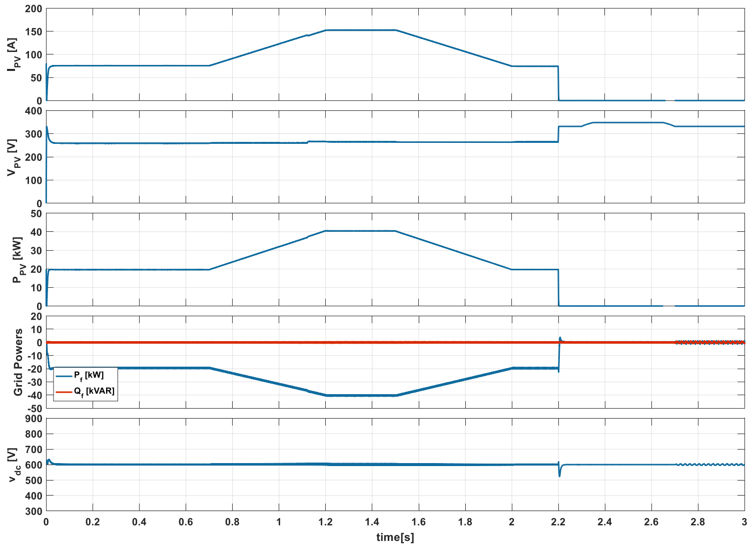

Figure 14. Simulation results of an open-switch fault in DC–DC converter without fault-tolerant topology

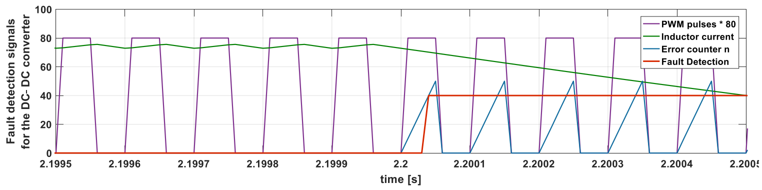

Figure 15. Fault detection signals for the DC–DC converter

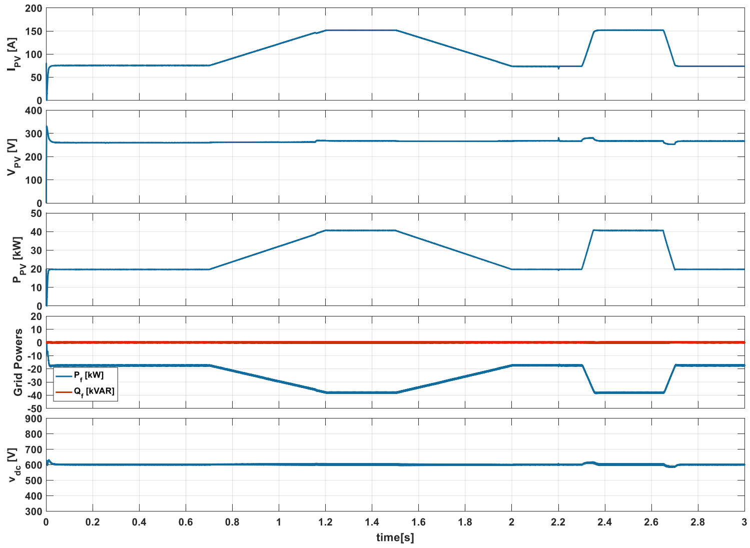

Figure 16. Simulation results of an open-switch fault in DC–DC converter with fault-tolerant topology

5.3. Case Study 3: GSC Open-Switch Fault Operation Mode

Figure 17 shows simulation results of studied system when an open-switch fault has occurred in GSC at the top switch of the leg number 1 (switch S_{g1}) at t=2.7s without fault-tolerant topology. The switch fault leads to high oscillations in grid active power P_f and grid reactive power Q_f, and consequently oscillations in the DC bus voltage v_{dc}. As a result, a high oscillation occurs in PV output voltage V_{PV}, PV output current I_{PV} and consequently PV output power P_{PV} as well. In summary, we can conclude that a failure in the GSC will endangers the overall system and leads to its stoppage.

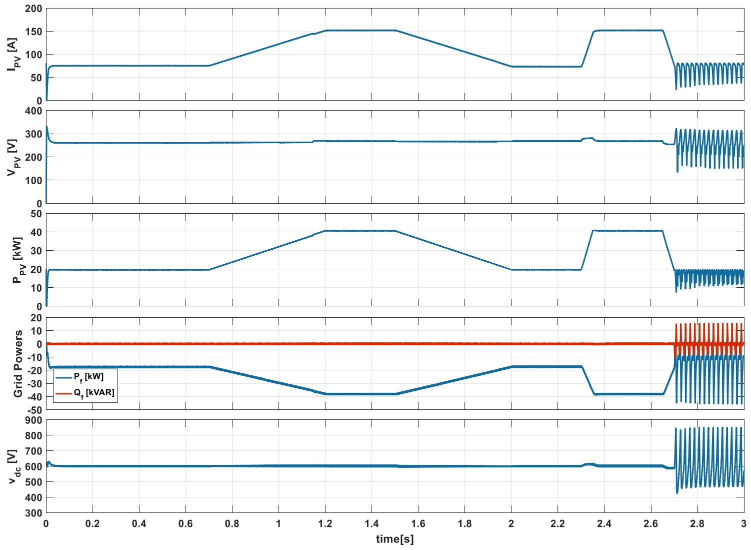

Figure 17. Simulation results of an open-switch fault in GSC without fault-tolerant topology

Figure 18, 19 and 20 show respectively, GSC measured voltage, GSC estimated voltage and GSC error voltage between measured and estimated voltages. We can see at Figure 20 that the error voltage is not null even before the switch fault occurrence, therefore, we need to filter it using mean value method.

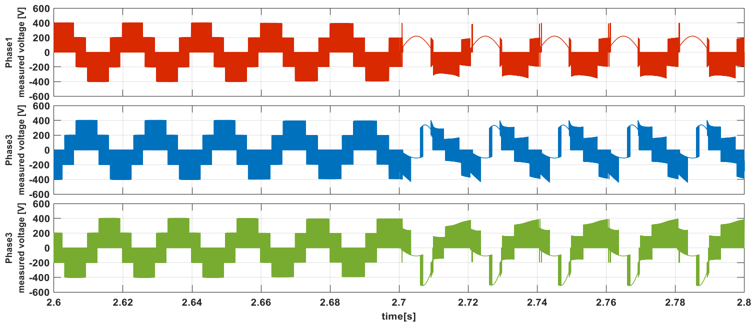

Figure 18. GSC measured voltage without fault-tolerant topology

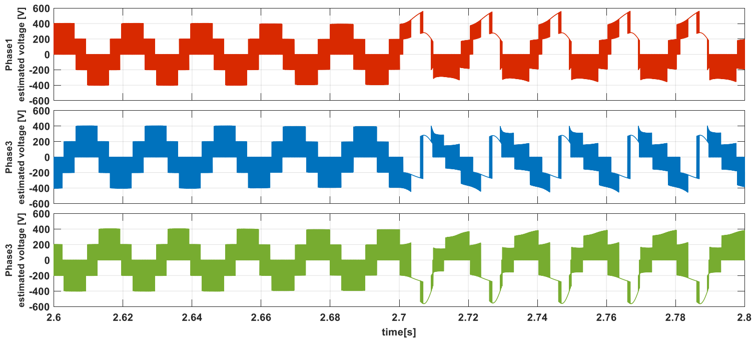

Figure 19. GSC estimated voltage without fault-tolerant topology

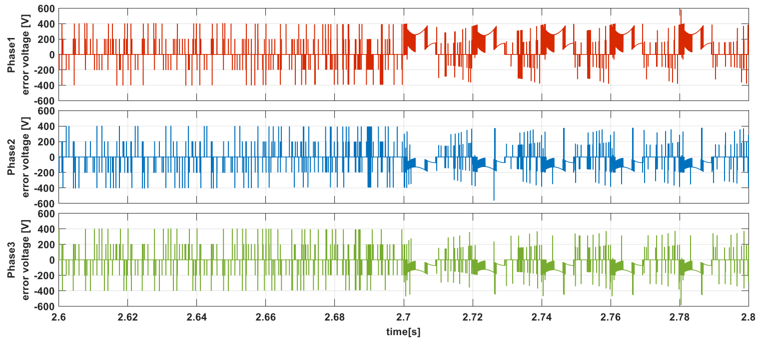

Figure 20. GSC error voltage without fault-tolerant topology

Figure 21 shows GSC error voltage mean value that used to detect the faulty leg. The fault detection time is t=2.70221s.

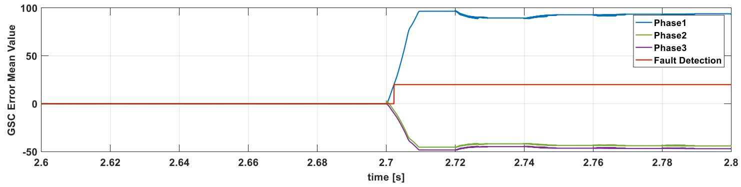

Figure 21. GSC error voltage mean value

Figure 22 shows simulation results for the same fault when the proposed fault-tolerant topology is used. One can see that the PV system can still operate in nominal conditions even after open-switch fault is occurred in GSC.

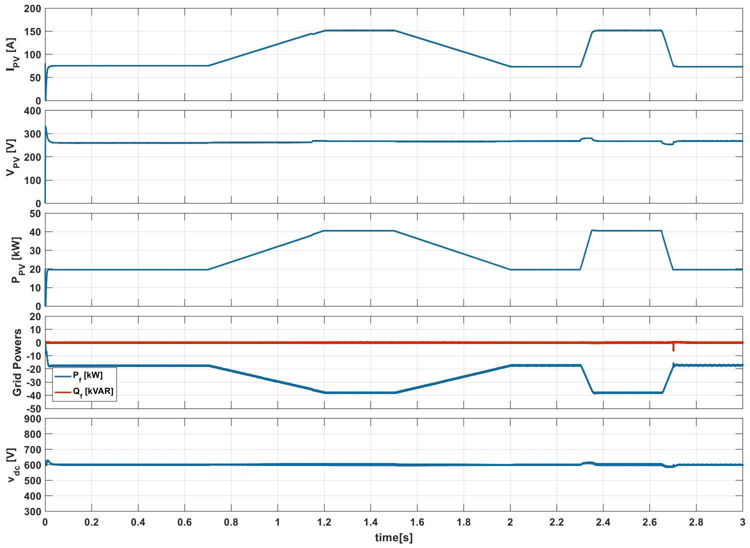

Figure 22. Simulation results of an open-switch fault in GSC with fault-tolerant topology

6. CONCLUSION

Open-switch fault-tolerant control of a grid-connected photovoltaic system for both DC–DC boost converter and grid-side converter (GSC) has been presented. The proposed fault tolerant control was validated by MATLAB/SIMULINK environment using the Simscape Power Systems toolbox. The fault-tolerant topology was achieved by adding one redundant switch to the unidirectional boost DC–DC converter, and by adding one redundant leg to the GSC. Moreover, we have proposed new fault detection methods for both power converters. The mean value of the error between measured and estimated simple voltages is used as fault indicator for the GSC, while, for the boost converter we have used the inductor current form as fault indicator. The proposed methods are fast and minimizes the delay time between the fault occurrence and its diagnosis. As proposed in this paper, the obtained results demonstrate that the grid-connected photovoltaic system can still operate in nominal conditions even after open-switch fault is occurred in both power converters, due to the proposed fault-tolerant control.

REFERENCES

[1] Bose B.K., "Global warming: energy, environmental pollution, and the impact of power electronics", *IEEE Industrial Electronics Magazine*, vol. 4, Issue 1, pp. 6-17, March, 2010.
[2] Bevrani, H., Ghosh, A., Ledwich, G., "Renewable energy sources and frequency regulation: survey and new perspectives", *IET Renewable Power Generation*, vol. 4, Issue 5, pp. 438-457, 2010.
[3] M. González, B. Raison, S. Bacha, L. Bun, "Fault Diagnosis in a Grid-Connected Photovoltaic System by Applying a Signal Approach", *IEEE Trans.Ind. Electron*., 978-1-61284-972-0, 2011.
[4] E. Ribeiro, A. Cardoso, C. Boccaletti, "Fault-Tolerant Strategy for a Photovoltaic DC–DC Converter", *IEEE Transactions on Power Electronics*, vol. 28, no. 6, June 2013.
[5] A. Ristow, M. Begovic, A. Pregeli, and A. Rohategi, "Development of amethodology for improving photovoltaic inverter reliability", *IEEE Trans.Ind. Electron*., vol. 55, no. 7, pp. 2581–2592, Jul. 2008.
[6] C. Wang, W. Chena, S. Shao, Z. Chen, B. Zhu, H. Li, "Energy Management of Stand-alone Hybrid PV System", Energy Procedia 12 (2011) 471 – 479.
[7] P. Bhatnagar, R.K. Nema, "Maximum power point tracking control techniques: State-of-the-art in photovoltaic applications", *Renewable and Sustainable Energy Reviews.*, 23, pp. 224–241, 2013.
[8] Ding K, Bian X-G, Liu H-H, Peng T. "A MATLAB-simulink-based PV module model and its application under conditions of nonuniform irradiance", *IEEE Trans Energy Convers*, vol. 27, no. 4, pp. 864–872, Dec 2012.
[9] Chung Henry Shu-Hung, *et al.*, "A novel maximum power point tracking technique for solar panels using a SEPIC or Cuk converter", *IEEE Transactions on Power Electronics*, vol. 18, no. 3, pp. 717–24, 2003.
[10] Femia Nicola, Petrone Giovanni, Spagnuolo Giovanni, Vitelli Massimo. "Optimization of perturb and observe maximum power point tracking method", *IEEE Transactions on Power Electronics*, vol. 20, no. 4, pp. 963–973, 2005.
[11] Femia N, Petrone G, Spagnuolo G, Vitelli M. "Increasing the efficiency of P&O MPPT by converter dynamic matching", *IEEE*, vol. 2, pp.1017–1021, 2004.
[12] A. Eid, "Utility integration of PV-wind-fuel cell hybrid distributed generation systems under variable load demands", *Electrical Power and Energy Systems* vol. 62, pp. 689–699, 2014.
[13] Kaygusuz A, Keles C, Alagoz BB, Karabiber A. "Renewable energy integration for smart cities," *Energy Build*, vol. 64, pp. 456–62, 2013.
[14] He J, Li YW, Munir MS. "A flexible harmonic control approach through voltage controlled DG-grid interfacing converters", *IEEE Trans Ind Electron*, vol. 59, no. 1, pp. 444–55, Jan 2012.
[15] Zhou T, Francois B. "Energy management and power control of a hybrid active wind generator for distributed power generation and grid integration", *IEEE Trans Ind Electron*, vol. 58, no. 1, pp. 95–104, 2011.
[16] S.V. Dhople, A. Davoudi, A.D. Dominguez-Garcia, and P.L. Chapman, "A unified approach to reliability assessment of multiphase DC–DC converters in photovoltaic energy conversion systems", *IEEE Trans. Power Electron.*, vol. 27, no. 2, pp. 739–751, Feb. 2012.
[17] G. Petrone, G. Spagnuolo, R. Teodorescu, M. Veerachary, and M. Vitelli, "Reliability issues in photovoltaic power processing systems", *IEEE Trans. Ind. Electron.*, vol. 55, no. 7, pp. 2569–2580, Jul. 2008.
[18] B. Lu and S.K. Sharma, "A literature review of IGBT fault diagnostic and protection methods for power inverters", *IEEE Trans. Ind. Appl*., vol. 45, no. 5, pp. 1770–1777, Sep.-Oct. 2009.
[19] K. Rothenhagen and F.W. Fuchs, *"Performance of diagnosis methods for IGBT open circuit faults in voltage source active rectifiers"*, in Proc. IEEE 35th Annu. Power Electron. Spec. Conf., vol. 6, pp. 4348–4354, Jun. 2004.
[20] P.S. Das and K.H. Kim, "Open-Switch Fault-Tolerant Control of a Grid-Side Converter in a Wind Power Generation System", *International Journal of Power Electronics and Drive System (IJPEDS)*, vol.6, no.2, pp.293-304, June 2015.
[21] M. Shahbazi, E. Jamshidpour, P. Poure, S. Saadate, M. Zolghadri, "Open- and Short-Circuit Switch Fault Diagnosis for Nonisolated DC–DC Converters Using Field Programmable Gate Array", *IEEE transactions on industrial electronics*, vol. 60, no. 9, September 2013.
[22] L. Benyettou, *et al.*, "Faults Diagnosis in Five-Level Three-Phase Shunt Active Power Filter", *International Journal of Power Electronics and Drive System (IJPEDS)*, vol. 6, no. 3, pp. 576- 585, September 2015.
[23] K. Ambusaidi, V. Pickert, and B. Zahawi, "New circuit topology for fault tolerant H-bridge DC–DC converter", *IEEE Trans. Power Electron.*, vol. 25, no. 6, pp. 1509–1516, Jun. 2010.
[24] S.Y. Kim, K. Nam, H.S. Song, and H.G. Kim, "Fault diagnosis of a ZVS DC–DC converter based on DC-link current pulse shapes", *IEEE Trans. Power Electron.*, vol. 55, no. 3, pp. 1491–1494, Mar. 2008.

[25] M. Shahbazi, M. Reza Zolghadri, Ph. Poure, S. Saadate, "Wind energy conversion system based on DFIG with Open Switch Fault Tolerant six-legs AC-DC-AC converter", *Industrial Technology (ICIT), 2013 IEEE International Conference on,* pp. 1656-1661, 2013.
[26] N.S. Ismail, I. Ahmad, H. Husain, and S. Chuah, *"Pulse power failure model of power MOSFET due to electrical overstress using Tasca method",* in Proc. IEEE Int. Conf. Semicond. Electron., Kuala Lumpur, Malaysia, pp. 1006–1009, 2006.

BIOGRAPHIES OF AUTHORS

Bilal Boudjellal was born in M'sila, Algeria. He received his License degree in Electromechanics from University of M'sila in 2011 and his Master degree in Electromechanical Systems Engineering from University of M'sila in 2013. His research interests include electrical drives control and diagnostic, power electronics, fault tolerant control, hardware implementation, renewable energy systems control, optimization and artificial intelligence.

Tarak Benslimane received the Engineer degree in Electrical Engineering from the University Center of Bechar (Algeria) in June 2001 and the Magister degree in electrical engineering from Military Polytechnic School of Algiers (Algeria) in February 2004. He received the Ph.D. degree in Electrical Engineering from Boumerdes University (Algeria), in 2009. Since 2009, he has held a teaching and research position in the Department of Electrical Engineering of M'sila University (Algeria), and he is still part of lecturing staff as Associate Professor. His scientific interests are power quality conditioning, power electronics, electrical drives control and diagnostic, fault tolerant control and renewable energies applications.